JSTT Journal of Science and Transport Technology

Journal of Science and Transport Technology
Journal homepage: https://jstt.vn/index.php/en

UNIVERSITY OF TRANSPORT TECHNOLOGY

Nonlinear buckling and postbuckling behaviors of porous FG-GPLRC cylindrical shells with stiffeners subjected to external pressure

Luu Ngoc Quang[1], Vu Minh Duc[2,3], Tran Quang Minh[4,*]
[1]Faculty of Civil Engineering, University of Transport Technology, Hanoi, Vietnam
[2]Laboratory of Advanced Materials and Structures, Institute for Advanced Study in Technology, Ton Duc Thang University, Ho Chi Minh City, Vietnam
[3]Faculty of Civil Engineering, Ton Duc Thang University, Ho Chi Minh City, Vietnam
[4]Institute of Transport Technology, University of Transport Technology, Hanoi, Vietnam

Article info
Type of article:
Original research paper

DOI:
https://doi.org/10.58845/jstt.utt.2024.en.4.2.24-36

[*]Corresponding author:
Email address:
minhtq@utt.edu.vn

Received: 01/06/2024
Revised: 17/06/2024
Accepted: 19/06/2024

Abstract: Buckling and postbuckling behaviors of porous functionally graded graphene platelets-reinforced composite (porous FG-GPLRC) cylindrical shells with stiffeners subjected to external pressures are presented in this paper. Three distribution types of porosity in the shells are considered. The smeared technique for stiffeners is employed to model the mechanical behaviors of the stiffened shells. The mechanical formulations are established by the thin shell theory considering large deflection assumption, and the Ritz method is applied for three deflection amplitudes. The postbuckling formula of the pressure-deflection and the explicit critical buckling pressures can be achieved. The numerical investigations indicate the outstanding effects of stiffeners, porosity distribution, porosity coefficient, and graphene platelet (GPL) mass fraction on the nonlinear buckling responses of the stiffened shells.

Keywords: Stiffener; External pressure; Porous Functionally graded graphene platelet reinforced composite; Cylindrical shell; Ritz energy method; Nonlinear buckling and postbuckling.

1. Introduction

The cylindrical shell is the typical case of closed shells applied for largely loaded structures. The composite materials can be used for this structure in a lot of applications in transport, civil, and aerospace technology equipment.

Functionally graded material (FGM) was manufactured to reduce the disadvantages of classical composite. In the last three decades, many researchers have made efforts to study on the dynamic and static problems of FGM shells. Postbuckling responses were investigated for FGM cylindrical shells with piezoelectric layers under external or hydrostatic pressures taking into account the higher-order shear deformation theory and singular perturbation method [1]. With the similar method and theory, the postbuckling responses of FGM cylindrical shells under internal pressure with the two-parameter foundation were studied [2]. By using the HSDT and neighboring balance criterion, the linear buckling responses of FGM cylindrical shells were studied [3]. The mixed boundary conditions and first-order shear deformation theory (FSDT) were considered in the vibrations and stability problems of FGM cylindrical shells under external pressure [4]. Torsional buckling and vibration of spirally stiffened and corrugated FGM cylindrical shells were mentioned using the thin shell theory [5,6].

A new type of FGM was created, namely, Functionally graded carbon nanotube reinforced composite (FG-CNTRC). The continuities and smoothness in mechanical properties of FG-CNTRC are designed by changing the volume fraction of carbon nanotubes (CNTs) through the thickness walls. Many studies show the remarkable behaviors of FG-CNTRC structures utilizing different methods and theories. Shen [7,8] studied the axially and pressure-loaded postbuckling responses of FG-CNTRC cylindrical shells with temperature rises. Linear buckling responses of FG-CNTRC toroidal shell segments and cylindrical shells with foundation interaction and subjected to axial compression and combined loads were investigated [9]. The skew FG-CNTRC cylindrical shells were considered in free vibration responses utilizing the Chebyshev-Ritz formulation [10]. The FG-CNTRC stiffeners were used to stiffen the FG-CNTRC cylindrical shells and the axial compressed buckling responses in thermal environment were investigated [11].

Other nanomaterials are graphene sheets (GSs) and graphene platelets (GPLs), and the new advanced composites are created from GSs and GPLs and isotropic material to be the Functionally Graded graphene reinforced composite (FG-GRC), and the Functionally Graded graphene platelets reinforced composite (FG-GPLRC). FG-GPLRC and FG-GRC surpass traditional materials due to their high tensile strength and rigidity, as well as excellent thermal and electrical conductivity. By utilizing GPLs and GSs, corrosion resistance and material longevity are enhanced, ideal for high-tech equipment in civil and mechanical engineering. Shen and Xiang [12,13] investigated the axially and pressure-loaded postbuckling responses of FG-GRC laminated cylindrical shells using the HSDT and two-step perturbation method. The FG-GRC laminated shells can be stiffened by FG-GRC laminated stiffeners and the torsionally, axially, and pressure-loaded cylindrical shells were studied using the Galerkin method [14-16]. The postbuckling responses of pressure-loaded FG-GRC laminated cylindrical shells with three-dimensional double-V meta-lattice auxetic core were presented [17]. Song et al. [18] investigated the low-velocity impact responses of FG-GPLRC plates using the modified nonlinear Hertz contact theory. Nonlinear buckling responses of FG-GPLRC circular plates and spherical caps with and without stiffeners were presented [19-21]. The higher-order shear deformable FG-GPLRC annular plates were considered in thermal vibration problems using the generalized differential quadrature method and Hamilton's principle [22]. Nonlinear torsional buckling responses of spirally stiffened FG-GPLRC cylindrical shells were presented [23] utilizing the improved smeared technique for stiffener and Donnell shell theory.

Porous materials are a common type of materials in application structures. With the small densities and large stiffnesses, porous materials were applied in many structures and mentioned in many research works. By distributing porosities into the FG-GPLRC structures, the advantages of both FG-GPLRC and porous materials can be utilized. Porous FG-GPLRC plates and shells were considered, and the effects of porosity and GPLs in the mechanical responses were discussed [24-26].

Stiffening with stiffeners improves the stiffness and load-carrying capacity of plates and shells without significantly increasing weight, optimizing material use in aerospace, automotive, and construction industries. As can be observed from open literature, there are no works studying the nonlinear buckling behaviors of the externally loaded porous FG-GPLRC cylindrical shells with stiffeners. Therefore, establishing the solutions for the problem of mechanical behavior of the FG-GPLRC shell with stiffeners is an important requirement for engineering design. An explicit solution of the nonlinear buckling pressures of these structures is presented in this paper. The nonlinear formulations are established by applying the Donnell shell, and nonlinear large deflection theories. The Ritz energy method is applied to investigate the postbuckling curves and critical buckling loads. The large effects of stiffeners, porosity distribution, porosity coefficient, and GPL mass fraction on the linear and nonlinear buckling behaviors of cylindrical shells are investigated in the numerical examples.

2. Porous FG-GPLRC cylindrical shells with stiffeners and governing expressions

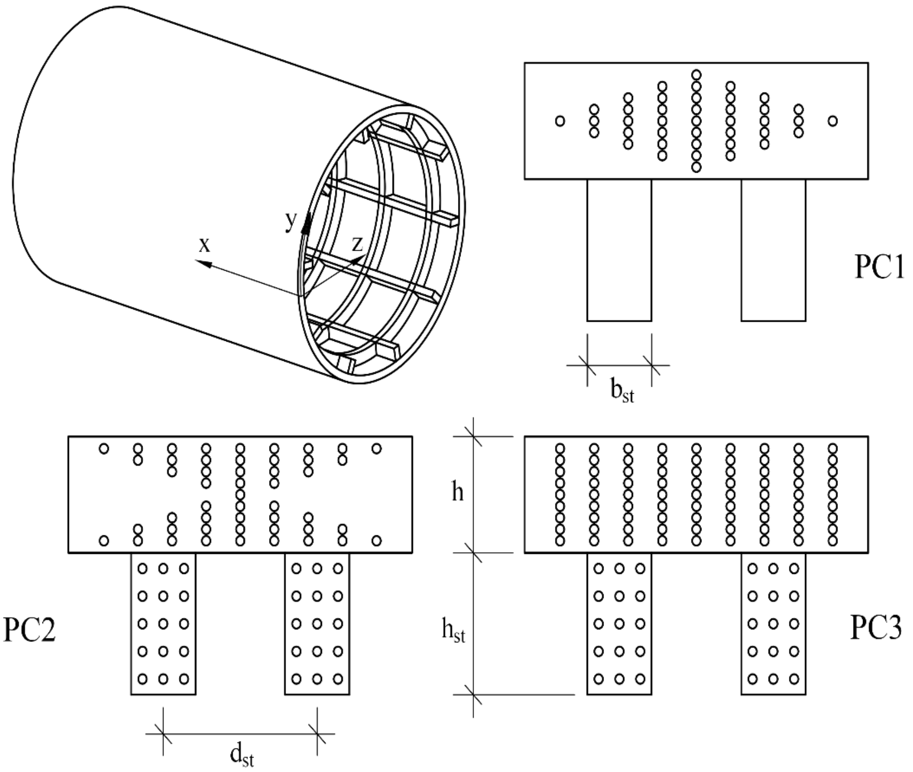

Fig. 1. Configuration and geometrical parameters of porous FG-GPLRC cylindrical shells with stiffeners

Consider the porous FG-GPLRC cylindrical shells with stiffeners under external pressure with uniform distributed pressure q_0. The geometrical parameters of shells and stiffeners are observed in Fig. 1. The radius and length of the shells are denoted by R and L, respectively.

In this paper, the distribution pattern of GPLs along the structure thickness is taken to be uniformly distributed type, the volume fraction of GPL can be expressed by

$$V_{GPL}^{*} = \frac{\rho_m W_{GPL}}{\rho_m W_{GPL} + \rho_{GPL}\left(1 - W_{GPL}\right)}. \quad (1)$$

The elastic modulus through the structure thickness can be estimated using the Halpin-Tsai model, meanwhile, the Poisson ratio is determined according to the mixture rule, as

$$E_1 = \frac{3E_m\left(1 + \Theta_G^L \Gamma_G^L V_{GPL}^{*}\right)}{8\left(1 - \Gamma_G^L V_{GPL}^{*}\right)} + \frac{5E_m\left(1 + \Theta_G^W \Gamma_G^W V_{GPL}^{*}\right)}{8\left(1 - \Gamma_G^W V_{GPL}^{*}\right)}, \quad (2)$$

$$\nu_1 = \nu_m V_m + \nu_{GPL} V_{GPL}^{*}, \quad (3)$$

where

$$\Gamma_G^L = \frac{E_{GPL} - E_m}{E_{GPL} + \Theta_G^L E_m},\ \Gamma_G^W = \frac{E_{GPL} - E_m}{E_{GPL} + \Theta_G^W E_m}, \quad \Theta_G^L = \frac{2a_{GPL}}{t_{GPL}},\ \Theta_G^W = \frac{2b_{GPL}}{t_{GPL}}, \quad (4)$$

with E, ν and ρ are the denotes of elastic modulus, Poisson ratio, and density, respectively. The subscripts GPL and m denote the GPL and matrix materials.

Three types of porosity distribution (PC1, PC2, and PC3) are considered in this paper, and the Poisson ratio and elastic modulus for the shells are expressed by

$$\nu_{sh} = \nu_1, \tag{5}$$

$$E_{sh} = \begin{cases} E_1\left[1-e_1\cos(\pi z/h)\right], & PC1 \\ E_1\left\{1-e_2\left[1-\cos(\pi z/h)\right]\right\}, & PC2 \\ E_1 e_3, & PC3 \end{cases} \tag{6}$$

and for the stiffeners

$$\nu_{st} = \nu_m, \tag{7}$$

$$E_{st} = \begin{cases} E_m, & PC1 \\ E_m(1-e_2), & PC2 \\ E_m e_3, & PC3 \end{cases} \tag{8}$$

where e_1, e_2, and e_3 are porosity coefficients.

It can be seen that the porosities are highly concentrated near the middle surface of the shell with PC1 distribution, on the contrary, they are concentrated mainly on the two shell surfaces with PC2 distribution, while evenly distributed over the shell thickness with PC3 distribution. The porosity distribution in the stiffeners is designed to ensure continuity between the shell and the stiffeners.

Considering the cases that the masses of the metal foam matrix are the same with different porosity distribution types, the following relations are applied as

$$\int_0^{h/2}\sqrt{1-e_1\cos(\pi z/h)}dz = \int_0^{h/2}\sqrt{1-e_2\left[1-\cos(\pi z/h)\right]}dz = \int_0^{h/2}\sqrt{e_3}dz, \tag{9}$$

where e_1 is chosen for the reference value, e_2 and e_3 are calculated according to e_1.

The Donnell shell and nonlinear large deflection theories are employed to establish the governing expressions of the buckling behaviors of stiffened cylindrical shells subjected to external pressures. The strain-displacement relations are derived in nonlinear forms, as

$$\varepsilon_x^0 = \frac{1}{2}w_{,x}^2 + u_{,x},\quad \varepsilon_y^0 = \frac{1}{2}w_{,y}^2 + v_{,y} - \frac{w}{R},\quad \gamma_{xy}^0 = w_{,x}w_{,y} + v_{,x} + u_{,y}. \tag{10}$$

The Hooke law for porous FG-GPLRC cylindrical shells is applied in this paper

$$\begin{bmatrix}\sigma_{11}\\ \sigma_{22}\\ \sigma_{12}\end{bmatrix} = \begin{bmatrix}Q_{11} & Q_{12} & 0\\ Q_{12} & Q_{22} & 0\\ 0 & 0 & Q_{66}\end{bmatrix}\begin{bmatrix}\varepsilon_{11}\\ \varepsilon_{22}\\ \gamma_{12}\end{bmatrix}. \tag{11}$$

The internal forces of the shells are derived in the forms

$$\begin{bmatrix}N_x\\ N_y\\ N_{xy}\\ M_x\\ M_y\\ M_{xy}\end{bmatrix} = \begin{bmatrix}D_{11} & D_{12} & 0 & C_{11} & C_{12} & 0\\ D_{12} & D_{22} & 0 & C_{12} & C_{22} & 0\\ 0 & 0 & D_{66} & 0 & 0 & C_{66}\\ C_{11} & C_{12} & 0 & B_{11} & B_{12} & 0\\ C_{12} & C_{22} & 0 & B_{12} & B_{22} & 0\\ 0 & 0 & C_{66} & 0 & 0 & B_{66}\end{bmatrix}\begin{bmatrix}\varepsilon_x^0\\ \varepsilon_y^0\\ \gamma_{xy}^0\\ -w_{,xx}\\ -w_{,yy}\\ -2w_{,xy}\end{bmatrix}, \tag{12}$$

where the components of stiffness D_{ij}, C_{ij}, and B_{ij} are calculated by

$$\left(D_{ij}, C_{ij}, B_{ij}\right) = \left(D_{ij}^{sh}, C_{ij}^{sh}, B_{ij}^{sh}\right) + \left(D_{ij}^{st}, C_{ij}^{st}, B_{ij}^{st}\right), \tag{13}$$

with $D_{ij}^{sh}, C_{ij}^{sh}, B_{ij}^{sh}$ and $D_{ij}^{st}, C_{ij}^{st}, B_{ij}^{st}$ are the stiffnesses of shell skin and stiffeners, as

$$\left(D_{ij}^{sh}, C_{ij}^{sh}, B_{ij}^{sh}\right) = \int_{h/2}^{-h/2} Q_{ij}\left(1, z, z^2\right)dz, \tag{14}$$

where

$$Q_{11} = E_{sh}\Big/\left(1-\nu_{sh}^2\right) = Q_{22},$$

$Q_{12} = E_{sh}\nu_{sh} \big/ \left(1 - \nu_{sh}^2\right)$, $Q_{66} = E_{sh} \big/ \left[2\left(1 + \nu_{sh}\right)\right]$.

The stiffnesses of stiffeners can be obtained using the improved smeared stiffener technique, by

$$D_{11}^{st} = \frac{b_{st}^x}{d_{st}^x} E_1^{stx},\ D_{22}^{st} = \frac{b_{st}^y}{d_{st}^y} E_1^{sty}, D_{12}^{st} = 0,$$
$$C_{11}^{st} = \frac{b_{st}^x}{d_{st}^x} E_2^{stx}, C_{22}^{st} = \frac{b_{st}^y}{d_{st}^y} E_2^{sty},\ C_{12}^{st} = 0, \quad (15)$$
$$B_{11}^{st} = \frac{b_{st}^x}{d_{st}^x} E_3^{stx},\ B_{22}^{st} = \frac{b_{st}^y}{d_{st}^y} E_3^{sty}, B_{12}^{st} = 0,$$
$$D_{66}^{st} = 0, \quad C_{66}^{st} = 0, \quad B_{66}^{st} = 0,$$

where

$$\left(E_1^{st}, E_2^{st}, E_3^{st}\right) = \int_{h/2}^{h/2+h_{st}} E_{st}\left(1, z, z^2\right) dz.$$

The deformation compatibility equation of porous FG-GPLRC cylindrical shells is established by employing Eq. (10), as

$$\varepsilon_{x,yy}^0 + \varepsilon_{y,xx}^0 - \gamma_{xy,xy}^0 - w_{,xy}^2 + \frac{w_{,xx}}{R} + w_{,yy}w_{,xx} = 0. \quad (16)$$

Introducing the stress function η with three following conditions, as

$$\eta_{,yy} = N_x, \quad \eta_{,xy} = -N_{xy}, \quad \eta_{,xx} = N_y. \quad (17)$$

By using Eqs. (10), (12) and (17), the compatibility equation (16) can be re-established in the following form

$$\left(D_{11}^* + D_{22}^* + D_{66}^*\right)\eta_{,xxyy} + D_{12}^*\eta_{,yyyy} - w_{,xy}^2 + D_{21}^*\eta_{,xxxx} + C_{21}^* w_{,xxxx} + C_{12}^* w_{,yyyy} + \frac{1}{R} w_{,xx} + \left(C_{11}^* + C_{22}^* - C_{66}^*\right) w_{,xxyy} + w_{,xx}w_{,yy} = 0, \quad (18)$$

where

$$D_{12}^* = \frac{D_{22}D_{66}}{\Omega}, D_{11}^* = -\frac{D_{12}D_{66}}{\Omega},$$
$$D_{22}^* = D_{11}^*,\ D_{66}^* = \frac{D_{11}D_{22} - D_{12}^2}{\Omega},\ D_{21}^* = \frac{D_{11}D_{66}}{\Omega},$$
$$C_{11}^* = D_{66}\frac{D_{22}C_{11} - D_{12}C_{12}}{\Omega},$$
$$C_{12}^* = D_{66}\frac{D_{22}C_{12} - D_{12}C_{22}}{\Omega},$$
$$C_{21}^* = D_{66}\frac{D_{11}C_{12} - D_{12}C_{11}}{\Omega},$$
$$C_{22}^* = D_{66}\frac{D_{11}C_{22} - D_{12}C_{12}}{\Omega},$$
$$C_{66}^* = 2C_{66}\frac{D_{11}D_{22} - D_{12}^2}{\Omega},$$
$$\Omega = D_{11}D_{22}D_{66} - D_{12}^2D_{66}.$$

3. Boundary conditions and solving method

The simply supported porous FG-GPLRC cylindrical shells with stiffeners under external pressure are considered. The boundary conditions at the ends can be presented by

$$w\big|_{x=0;x=L} = M_x\big|_{x=0;\,x=L} = N_x\big|_{x=0;x=L} = N_{xy}\big|_{x=0;x=L} = 0. \quad (19)$$

The popular form of deflection of pressured cylindrical shells is chosen approximately by

$$w(x,y) = f_0 + f_1 \sin\frac{m\pi x}{L}\sin\frac{ny}{R} + f_2\sin^2\frac{m\pi x}{L}, \quad (20)$$

Where f_0, f_1 and f_2 are the deflection amplitudes, m and n are the buckling modes of shells.

By substituting Eq. (20) into Eq. (18), the stress function can be achieved, leads to

$$\eta = \eta_1\sin\frac{m\pi x}{L}\sin\frac{ny}{R} + \eta_2\cos\frac{2m\pi x}{L} + \eta_3\sin\frac{3m\pi x}{L}\sin\frac{ny}{R} + \eta_4\cos\frac{2ny}{R} - \sigma_{0y}\frac{hx^2}{2}, \quad (21)$$

where σ_{0y} is the circumferential stress, and

$$\eta_1 = \frac{\kappa_1}{\kappa_3}f_1 + \frac{\kappa_2}{\kappa_3}f_1f_2, \quad \eta_3 = \frac{\kappa_4}{\kappa_5}f_1f_2,$$
$$\eta_2 = \frac{1}{2}\frac{C_{21}^*}{D_{21}^*}f_2 - \frac{1}{8}\frac{L^2}{Rm^2\pi^2D_{21}^*}f_2 + \frac{1}{32}\frac{L^2n^2}{m^2\pi^2R^2D_{21}^*}f_1^2,$$
$$\eta_4 = \frac{1}{32}\frac{m^2\pi^2R^2}{L^2n^2D_{12}^*}f_1^2,$$
$$\kappa_1 = -\frac{\pi^8m^8}{L^8}D_{21}^*C_{21}^* - \frac{n^8}{R^8}D_{12}^*C_{12}^*$$

$$-\frac{m^6\pi^6n^2}{L^6R^2}\begin{bmatrix}\left(C^*_{11}-C^*_{66}+C^*_{22}\right)D^*_{21}\\+\left(D^*_{11}+D^*_{66}+D^*_{22}\right)C^*_{21}\end{bmatrix}-$$

$$\frac{m^4\pi^4n^4}{L^4R^4}\begin{bmatrix}\left(D^*_{22}+D^*_{11}+D^*_{66}\right)\left(C^*_{22}+C^*_{11}-C^*_{66}\right)\\+C^*_{21}D^*_{12}+D^*_{21}C^*_{12}\end{bmatrix}+$$

$$\left(\frac{m^4\pi^4n^2}{L^4R^2a}+\frac{\pi^6m^6}{L^6R}\right)D^*_{21}+\left(\frac{m^2\pi^2n^4}{L^2R^5}+\frac{n^6}{aR^6}\right)D^*_{12}$$

$$+\left(\frac{m^2\pi^2n^4}{aL^2R^4}+\frac{m^4\pi^4n^2}{L^4R^3}\right)\left(D^*_{11}+D^*_{22}+D^*_{66}\right)$$

$$-\frac{m^2\pi^2n^6}{L^2R^6}\begin{bmatrix}\left(C^*_{11}-C^*_{66}+C^*_{22}\right)D^*_{12}\\+\left(D^*_{11}+D^*_{66}+D^*_{22}\right)C^*_{12}\end{bmatrix},$$

$$\kappa_3=\begin{bmatrix}\frac{\pi^4m^4}{L^4}D^*_{21}+\frac{n^4}{R^4}D^*_{12}\\+\frac{m^2\pi^2n^2}{L^2R^2}\left(D^*_{11}+D^*_{22}+D^*_{66}\right)\end{bmatrix}^2,$$

$$\kappa_4=81\frac{m^6\pi^6n^2}{L^6R^2}D^*_{21}+\frac{m^2\pi^2n^6}{L^2R^6}D^*_{12}$$
$$+9\frac{m^4\pi^4n^4}{L^4R^4}\left(D^*_{11}+D^*_{22}+D^*_{66}\right),$$

$$\kappa_2=-\frac{m^6n^2\pi^6}{L^6R^2}D^*_{21}$$
$$-\frac{m^4\pi^4n^4}{L^4R^4}\left(D^*_{11}+D^*_{22}+D^*_{66}\right)-\frac{m^2\pi^2n^6}{L^2R^6}D^*_{12},$$

$$\kappa_5=\begin{bmatrix}81\frac{m^4\pi^4}{L^4}D^*_{21}+\frac{n^4}{R^4}D^*_{12}\\+9\frac{m^2\pi^2n^2}{L^2R^2}\left(D^*_{11}+D^*_{22}+D^*_{66}\right)\end{bmatrix}^2.$$

For cylindrical shells, the circumferentially closed condition must be satisfied, presented as

$$\int_0^{2\pi R}\int_0^{L}v_{,y}dxdy=\int_0^{2\pi R}\int_0^{L}\left(\varepsilon^0_y+\frac{w}{R}-\frac{1}{2}w^2_{,y}\right)dxdy=0. \quad (22)$$

Eq. (22) can be rewritten using Eqs. (10) and (12), as

$$\sigma_{0y}=\frac{1}{D^*_{21}}\left(\frac{1}{Rh}f_0-\frac{n^2}{8R^2h}f_1^2+\frac{1}{2Rh}f_2\right). \quad (23)$$

The potential energy is derived as

$$U=-\int_0^{L}\int_0^{2\pi R}q_0wdxdy$$
$$+\frac{1}{2}\int_{-\frac{h}{2}}^{\frac{h}{2}}\int_0^{2\pi R}\int_0^{L}\left(\varepsilon_x\sigma_x+\varepsilon_y\sigma_y+\gamma_{xy}\tau_{xy}\right)dxdydz. \quad (24)$$

The potential energy is re-established according to two unknown functions to be deflection w and stress function η. Substituting the stress function and deflection forms in Eqs. (20) and (21) to the new form of the total energy, finally, applying the Ritz method, as

$$\frac{\partial U}{\partial f_0}=\frac{\partial U}{\partial f_1}=\frac{\partial U}{\partial f_2}=0. \quad (25)$$

Combining Eq. (25) with the circumferentially closed condition (22), leads to

$$\lambda_{11}f_0+\lambda_{12}f_1^2+\lambda_{13}f_2-2q_0=0, \quad (26)$$

$$\lambda_{21}f_0+\lambda_{22}f_1^2+\lambda_{23}f_2^2+\lambda_{24}f_2+\lambda_{26}=0, \quad (27)$$

$$\lambda_{31}f_0+\lambda_{32}f_1^2+\lambda_{33}f_1^2f_2+\lambda_{34}f_2-q_0=0, \quad (28)$$

where

$$\lambda_{11}=\frac{2}{R^2D^*_{21}},\quad \lambda_{12}=-\frac{n^2}{4R^3D^*_{21}},$$

$$\lambda_{13}=\frac{1}{R^2D^*_{21}},\quad \lambda_{14}=-\frac{h\left(D^*_{11}+D^*_{22}\right)}{RD^*_{21}},$$

$$\lambda_{21}=2S_5,\ \lambda_{22}=2S_1,\ \lambda_{23}=2S_2,$$

$$\lambda_{24}=2S_3,\ \lambda_{25}=2S_6-\frac{\pi^2hm^2}{L^2}+\frac{n^2h}{R^2}\frac{D^*_{11}}{D^*_{21}},$$

$$\lambda_{26}=2S_4,\lambda_{31}=T_4,\ \lambda_{32}=T_2,\ \lambda_{33}=T_1,$$

$$\lambda_{34}=T_3,\ \lambda_{35}=-\frac{\pi^2hm^2}{L^2},\ \lambda_{36}=T_5-\frac{hD^*_{11}}{RD^*_{21}},$$

$$S_1=\frac{1}{32}\left(\frac{\pi^4m^4}{L^4D^*_{12}}+\frac{3n^4}{R^4D^*_{21}}\right),$$

$$S_2 = \frac{9}{2}\left(\frac{\kappa_4{}^2}{\kappa_5{}^2}\right)R_2 + \frac{1}{2}\left(\frac{\kappa_2{}^2}{\kappa_3{}^2}\right)R_1,$$

$$S_3 = \frac{\kappa_1\kappa_2}{\kappa_3{}^2}R_1 + \frac{1}{2}\frac{\kappa_2(R_5+R_8)}{\kappa_3} + \frac{1}{4}\frac{\pi^2m^2n^2\left(J_{11}+C^*_{21}\right)}{L^2R^2D^*_{21}} - \frac{3}{8}\frac{n^2}{R^3D^*_{21}},$$

$$S_4 = \frac{1}{2}\left(\frac{\kappa_1{}^2}{\kappa_3{}^2}\right)R_1 + \frac{1}{2}\frac{\kappa_1(R_5+R_8)}{\kappa_3} - \frac{1}{2}\frac{n^4G_{22}}{R^4} - \frac{1}{2}\frac{\pi^2m^2n^2\left(2G_{66}+G_{21}+G_{12}\right)}{R^2L^2} - \frac{1}{2}\frac{\pi^4m^4G_{11}}{L^4},$$

$$S_5 = -\frac{1}{2}\frac{n^2}{R^3D^*_{21}}, \qquad S_6 = -\frac{1}{4}\frac{hn^2\left(D^*_{11}-D^*_{22}\right)}{R^2D^*_{21}},$$

$$T_1 = \frac{9}{2}\frac{\kappa_4{}^2}{\kappa_5{}^2}R_2 + \frac{1}{2}\frac{\kappa_2{}^2}{\kappa_3{}^2}R_1,$$

$$T_4 = \frac{1}{R^2D^*_{21}}, \quad T_5 = \frac{h\left(D^*_{11}-D^*_{22}\right)}{2RD^*_{21}},$$

$$T_2 = \frac{1}{2}\frac{\kappa_1\kappa_2}{\kappa_3{}^2}R_1 + \frac{1}{4}\frac{\kappa_2(R_5+R_8)}{\kappa_3} + \frac{1}{8}\frac{\pi^2m^2n^2\left(J_{11}+C^*_{21}\right)}{R^2L^2D^*_{21}} - \frac{3}{16}\frac{n^2}{R^3D^*_{21}},$$

$$T_3 = \frac{3}{4R^2D^*_{21}} - \frac{\pi^2m^2}{L^2R}\frac{C^*_{21}+J_{11}}{D^*_{21}} + 4\frac{\pi^4m^4}{L^4}\left(\frac{J_{11}C^*_{21}}{D^*_{21}} - G_{11}\right),$$

$$R_1 = \frac{n^2\pi^2m^2}{L^2R^2}\left(D^*_{11}+D^*_{22}+D^*_{66}\right) + \frac{n^4}{R^4}D^*_{12} + \frac{\pi^4m^4}{L^4}D^*_{21},$$

$$R_5 = \frac{m^2n^2\pi^2\begin{pmatrix}C^*_{11}+C^*_{22}-C^*_{66}\\ -J_{21}-J_{12}-2J_{66}\end{pmatrix}}{R^2L^2},$$

$$R_2 = \frac{n^2\pi^2m^2}{L^2R^2}\left(D^*_{11}+D^*_{22}+D^*_{66}\right) + \frac{1}{9}\frac{n^4}{R^4}D^*_{12} + 9\frac{\pi^4m^4}{L^4}D^*_{21},$$

$$R_8 = \frac{n^4\left(C^*_{12}-J_{22}\right)}{R^4} + \frac{m^4\pi^4\left(C^*_{21}-J_{11}\right)}{L^4},$$

$$J_{11} = C_{11}D^*_{11} + C_{12}D^*_{21},\ J_{12} = C_{11}D^*_{12} + C_{12}D^*_{22},$$

$$J_{21} = C_{21}D^*_{11} + C_{22}D^*_{21},\ J_{22} = C_{21}D^*_{12} + C_{22}D^*_{22},$$

$$J_{66} = -C_{66}D^*_{66},\ \ G_{11} = C_{11}C^*_{11} + C_{12}C^*_{21} - B_{11},$$

$$G_{12} = C_{11}C^*_{12} + C_{12}C^*_{22} - B_{12},$$

$$G_{21} = C_{21}C^*_{11} + C_{22}C^*_{21} - B_{21},$$

$$G_{22} = C_{21}C^*_{12} + C_{22}C^*_{22} - B_{22},$$

$$G_{66} = C_{66}C^*_{66} - 2B_{66}.$$

By totalling three deflection amplitudes, the maximum deflection is calculated, and that is written by the amplitude f_2, as

$$W_{max} = f_0 + f_1 + f_2 = \frac{\lambda_{12}\lambda_{23}}{\lambda_{11}\lambda_{22}-\lambda_{12}\lambda_{21}}f_2{}^2 + \frac{\lambda_{12}\lambda_{24}-\lambda_{13}\lambda_{22}}{\lambda_{11}\lambda_{22}-\lambda_{12}\lambda_{21}}f_2 + \frac{2\lambda_{22}}{\lambda_{11}\lambda_{22}-\lambda_{12}\lambda_{21}}q_0 + \frac{\lambda_{12}\lambda_{26}}{\lambda_{11}\lambda_{22}-\lambda_{12}\lambda_{21}} + \left[-\frac{\lambda_{23}\lambda_{11}}{\lambda_{11}\lambda_{22}-\lambda_{12}\lambda_{21}}f_2{}^2 - \frac{\lambda_{11}\lambda_{24}-\lambda_{13}\lambda_{21}}{\lambda_{11}\lambda_{22}-\lambda_{12}\lambda_{21}}f_2 - \frac{2\lambda_{21}}{\lambda_{11}\lambda_{22}-\lambda_{12}\lambda_{21}}q_0 - \frac{\lambda_{11}\lambda_{26}}{\lambda_{11}\lambda_{22}-\lambda_{12}\lambda_{21}}\right]^{\frac{1}{2}} + f_2. \tag{29}$$

The amplitudes f_0 and f_2 are achieved from Eqs. (26) and (28), then substituting these amplitudes into Eq. (27), one can be obtained by

$$q_0 = -\frac{\delta_{11}f_2{}^3 + \delta_{12}f_2{}^2 + \delta_{13}f_2 + \delta_{18}}{\delta_{15}f_2 + \delta_{17}}, \tag{30}$$

where

$$\delta_{10} = 1/\left(\lambda_{22}\lambda_{11} - \lambda_{21}\lambda_{12}\right),\ \delta_{11} = -\lambda_{33}\lambda_{23}\lambda_{11}\delta_{10},$$

$$\delta_{12} = \begin{bmatrix}\lambda_{33}\left(\lambda_{13}\lambda_{21}-\lambda_{11}\lambda_{24}\right)\\ +\left(\lambda_{31}\lambda_{12}-\lambda_{32}\lambda_{11}\right)\lambda_{23}\end{bmatrix}\delta_{10},$$

$$\delta_{13} = \begin{bmatrix}\left(\lambda_{21}\lambda_{32}-\lambda_{22}\lambda_{31}\right)\lambda_{13}\\ +\left(\lambda_{24}\lambda_{31}-\lambda_{21}\lambda_{34}\right)\lambda_{12}\\ +\left(\lambda_{22}\lambda_{34}-\lambda_{24}\lambda_{32}-\lambda_{26}\lambda_{33}\right)\lambda_{11}\end{bmatrix}\delta_{10},$$

$$\delta_{15} = -2\lambda_{33}\lambda_{21}\delta_{10},$$

$$\delta_{14} = \begin{bmatrix}\left(\lambda_{14}\lambda_{33}-\lambda_{12}\lambda_{35}\right)\lambda_{21}\\ +\left(\lambda_{22}\lambda_{35}-\lambda_{25}\lambda_{33}\right)\lambda_{11}\end{bmatrix}\delta_{10},$$

$$\delta_{16} = \begin{bmatrix} (\lambda_{21}\lambda_{32} - \lambda_{22}\lambda_{31})\lambda_{14} \\ +(\lambda_{25}\lambda_{31} - \lambda_{21}\lambda_{36})\lambda_{12} \\ +(\lambda_{22}\lambda_{36} - \lambda_{25}\lambda_{32})\lambda_{11} \end{bmatrix}\delta_{10},$$

$$\delta_{17} = \left[(\lambda_{12} - 2\lambda_{32})\lambda_{21} - \lambda_{22}(\lambda_{11} - 2\lambda_{31})\right]\delta_{10},$$

$$\delta_{18} = \lambda_{26}(\lambda_{12}\lambda_{31} - \lambda_{11}\lambda_{32})\delta_{10}.$$

The postbuckling curve $W_{max} - q_0$ is determined by combining the $W_{max} - f_2$ and $q_0 - f_2$ relations. By applying $f_2 \to 0$ in Eq. (30), the upper buckling pressures of the stiffened shells are achieved as

$$q_0^{upper} = -\frac{\delta_{18}}{\delta_{17}}. \quad (31)$$

The critical buckling pressures q_0^{cr} can be obtained to be minimal values of upper buckling pressures for all buckling modes m and n.

4. Numerical examples

The accuracy of the present results can be evaluated by the comparisons of the critical external buckling pressure with those of previous work [2]. The validations of the critical external pressured buckling loads of FGM cylindrical shells with various volume fraction indexes of FGM are presented in Table 1. Clearly, the accuracy of the present results is confirmed from these validations.

To elucidate the theoretical results of this algorithm, the stiffened cylindrical shells are made from the copper matrix porous FG-GPLRC. The parameters of materials can be chosen by Wang et al. [22]. Due to the dominance of critical buckling modes, the buckling load and postbuckling curve below are all investigated at the critical modes.

Table 2 investigates the critical buckling loads of unstiffened and stiffened porous FG-GPLRC shells with various porosity distributions and porosity coefficients. Due to the porosity distribution mainly in the middle surface area of the shell, the stiffnesses of the PC1 shell is the largest and the largest critical buckling loads can be obtained in the investigated results. The very strong influences of stiffeners are inspected in this Table. As observed in Eq. (8), the elastic modulus of the stiffeners of the PC1 shell is the largest, leading to the superiority of the critical buckling load of the PC1 stiffened shell compared to the other two distributions. Additionally, the critical buckling loads of the shells decrease as the porosity coefficient increases, slightly decreasing for the PC1 distribution and largely for the PC2 and PC3 distributions. The results also show that the critical pressures of PC1 shells are the largest and those of PC2 are the smallest.

Effects of stiffeners on the postbuckling responses of porous FG-GPLRC cylindrical shells with stiffeners are presented in Fig. 2. The differences between the postbuckling curves of orthogonally stiffened shells and unstiffened shells are presented in Fig. 2a, between the postbuckling curves of orthogonally stiffened shells and stringer stiffened shells are shown in Fig. 2b, and between the postbuckling curves of orthogonally stiffened shells and ring stiffened shells are presented in Fig. 2c. Due to the complex nonlinear characteristics and different critical buckling modes, it can be seen in Figs. 2a and 2b that the load-carrying capacity of the shell with orthogonal and stringer stiffeners, respectively, is superior to that of the unstiffened shell when the deflection is small, however, when the deflection is large enough, the opposite trend can be observed. The large different between postbuckling curves can be observed for the case of orthogonally stiffened and unstiffened shells, and for the case of orthogonally stiffened and stringer stiffened shells, oppositely, for the case of orthogonally stiffened and ring stiffened shells. Snap-through phenomenon can be clearly observed for the cases of orthogonal stiffened and ring stiffened shells, and slightly observed for the case of stringer stiffened and unstiffened shells. Effects of distance between stiffeners, stiffener widths, and stiffener heights are investigated in Figs. 2d, e, and f, respectively. As can be seen, the largest effects are obtained as the change of the stiffener height.

Effects of geometrical and material properties on the postbuckling responses of porous FG-GPLRC cylindrical shells with stiffeners are shown in Fig. 3. Fig. 3a presents the shell length on the postbuckling curve of stiffened shells. Clearly, the critical buckling load largely decreases as the shell length increases. The large effects of porosity coefficient, porosity distribution, and GPL mass fraction on the postbuckling curve of the shells can be observed in Figs. 3b, c, and d. While the regular tendency of postbuckling curves with the same buckling modes $(m,n)=(1,6)$ are observed as the porosity coefficient changes (Fig. 3b), a complex tendency is obtained as the porosity distribution and GPL mass fraction change (Figs. 3c, d) with two different buckling modes (m,n).

Table 1. Comparisons of critical buckling loads $\overline{q}_0^{cr} = q_0^{cr}h$ (kPa.m) of FGM cylindrical shells with different geometrical parameters ($R/h=400$, h=1mm, $L=\sqrt{500Rh}$)

N	0.2	1	2	5
Shen et al. [2]	81.3248(1,11)*	71.1508(1,11)	67.3886(1,11)	63.7561(1,11)
Present	89.2169(1,11)	75.5062(1,11)	70.4914(1,11)	65.8170(1,11)

* The critical buckling modes (m,n)

Table 2. The critical buckling loads of porous FG-GPLRC stiffened cylindrical shells with different porosity distributions and porosity coefficients (MPa, $L/R=1.5$, h=0.04m, $R/h=100$, W_{GPL}=0.6%, $h_{st}^x = h_{st}^y = 1.5h$, $b_{st}^x = b_{st}^y = h$, $d_{st}^x = d_{st}^y = 5h$)

	e_1	0	0.1	0.2	0.3	0.5
Unstiffened	PC1	1.178(1,7)	1.129(1,7)	1.080(1,7)	1.030(1,7)	0.932(1,7)
	PC2	1.178(1,7)	1.059(1,7)	0.942(1,7)	0.828(1,7)	0.613(1,7)
	PC3	1.178(1,7)	1.103(1,7)	1.027(1,7)	0.950(1,7)	0.793(1,7)
Orthogonally stiffened	PC1	3.779(1,6)	3.687(1,6)	3.592(1,6)	3.477(1,5)	3.174(1,5)
	PC2	3.779(1,6)	3.275(1,6)	2.769(1,6)	2.262(1,6)	1.251(1,6)
	PC3	3.779(1,6)	3.538(1,6)	3.294(1,6)	3.048(1,6)	2.544(1,6)

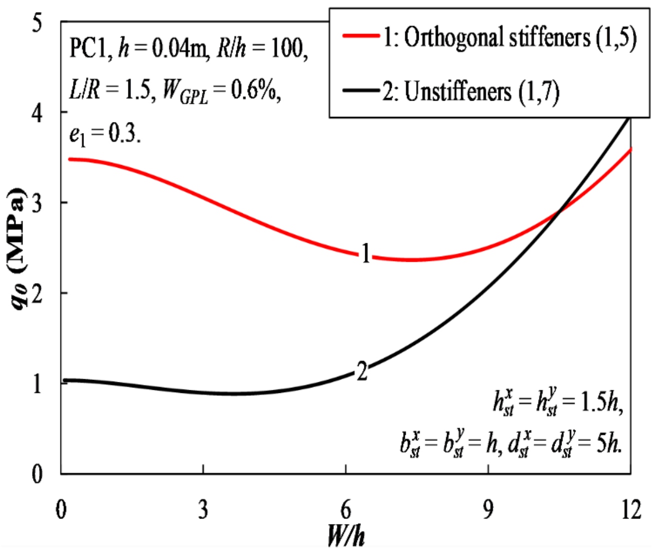

(a)

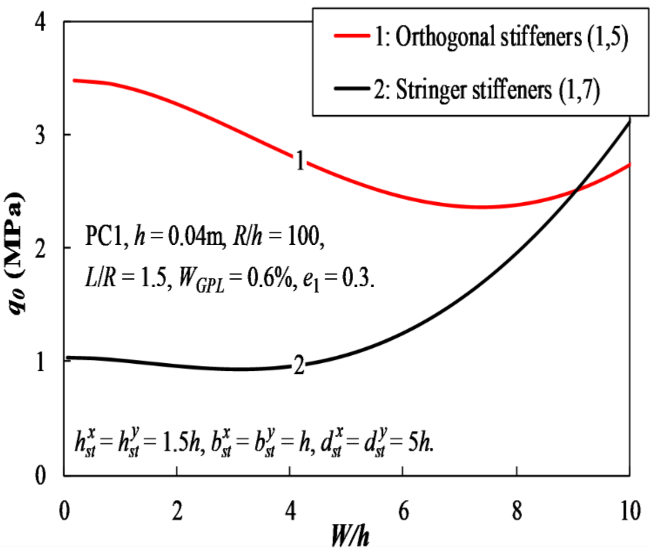

(b)

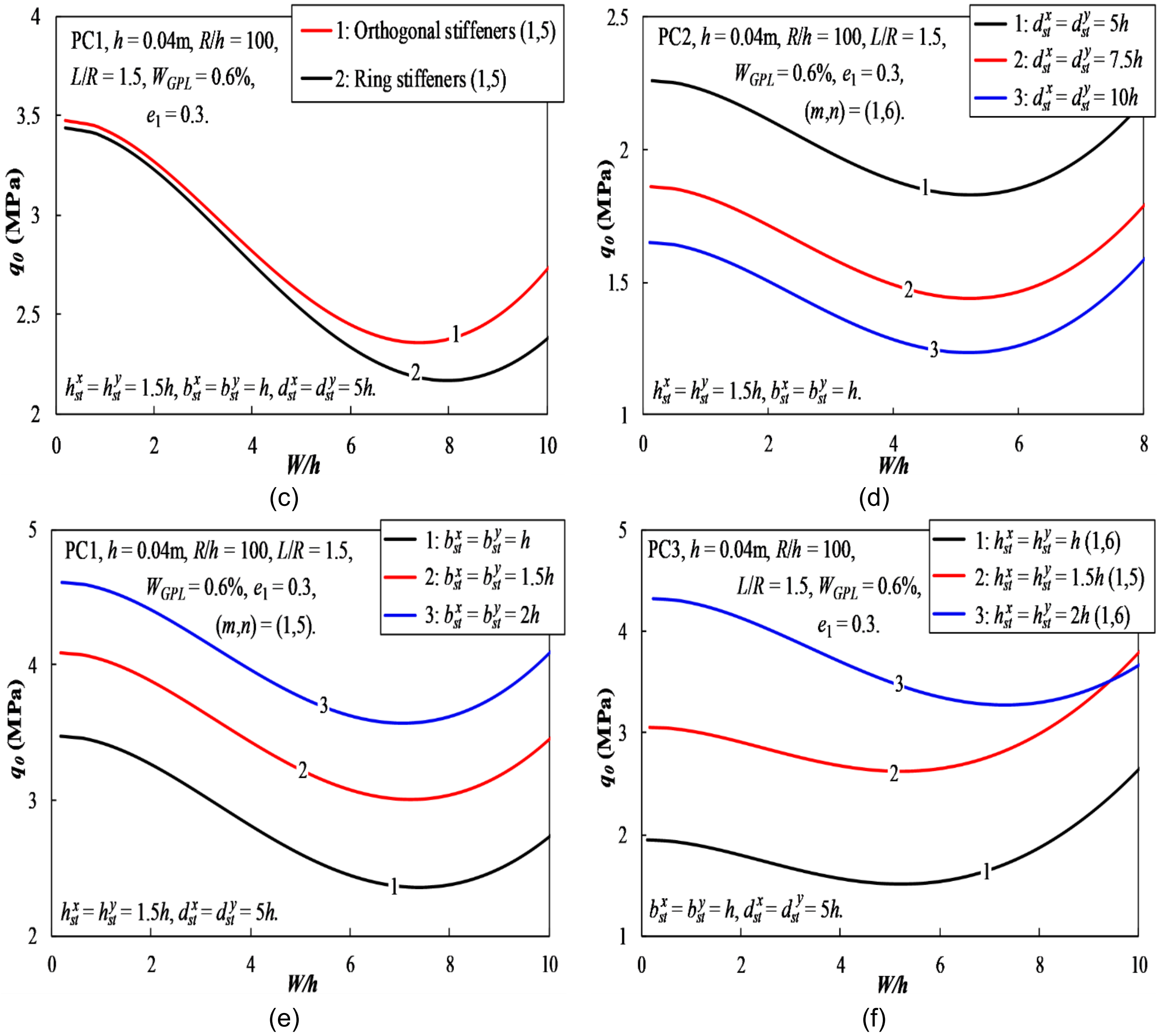

Fig. 2. Effects of stiffeners on the postbuckling responses of porous FG-GPLRC cylindrical shells

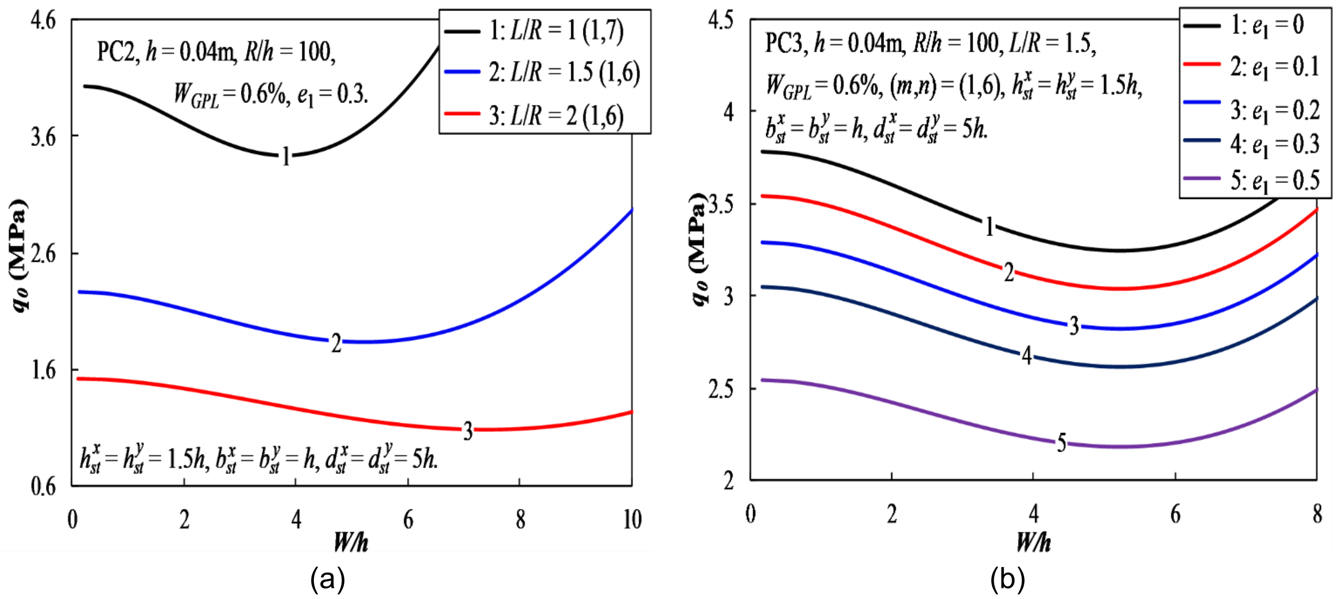

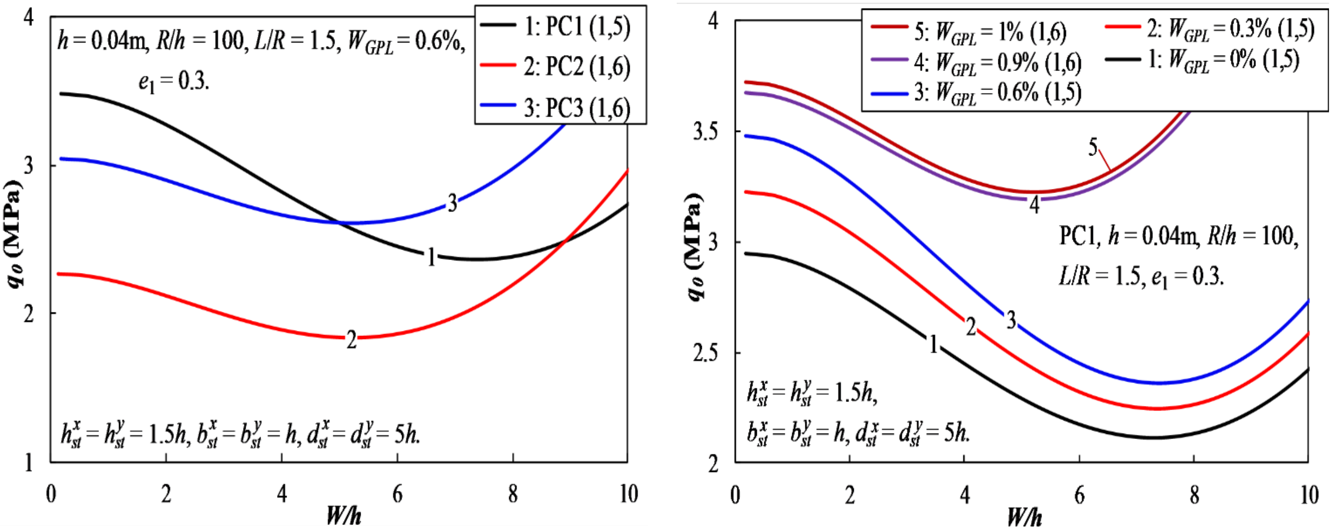

(c) (d)

Fig. 3. Effects of geometrical and material properties on the postbuckling responses of porous FG-GPLRC cylindrical shells with stiffeners

5. Concluding remarks

To predict the influences of the stiffeners on the buckling behaviors of the porous FG-GPLRC cylindrical shells subjected to the external pressures, an analytical approach to buckling and postbuckling problems is established by summing the stiffnesses of stiffeners with those of shell skin. The smeared stiffener technique is applied and the Ritz energy method is used. Some outstanding remarks can be achieved as

1) The stiffeners greatly affect the critical pressures and postbuckling pressure behaviors of the considered structures.

2) Snap-through phenomenon is clearly observed for the cases of orthogonal stiffened and ring stiffened shells, and more slightly observed for the cases of stringer stiffened and unstiffened shells.

3) The large effects of porosity coefficient, porosity distribution, and GPL mass fraction on the critical buckling load and postbuckling curve of the shells can be observed

References

[1]. H.S. Shen, N. Noda. (2007). Postbuckling of pressure-loaded FGM hybrid cylindrical shells in thermal environments. *Composite Structures*, 77(4), 546-560.

[2]. H.S. Shen, J. Yang, S. Kitipornchai. (2010). Postbuckling of internal pressure loaded FGM cylindrical shells surrounded by an elastic medium. *European Journal of Mechanics - A/Solids*, 29(3), 448-460.

[3]. E. Bagherizadeh, Y. Kiani, M.R. Eslami. (2011). Mechanical buckling of functionally graded material cylindrical shells surrounded by Pasternak elastic foundation. *Composite Structures*, 93(11), 3063-3071.

[4]. A. H. Sofiyev, D. Hui. (2019). On the vibration and stability of FGM cylindrical shells under external pressures with mixed boundary conditions by using FOSDT. *Thin-Walled Structures*, 134, 419-427.

[5]. N.T. Phuong, D.T. Luan, V.H. Nam, P.T. Hieu. (2019). Nonlinear approach on torsional buckling and postbuckling of functionally graded cylindrical shells reinforced by orthogonal and spiral stiffeners in thermal environment. *Proceedings of the Institution of Mechanical Engineers, Part C: Journal of Mechanical Engineering Science*, 233(6), 2091-2106.

[6]. N.T. Phuong, N.T. Trung, T.D. Kien, H.D. Tuan, V.H. Nam. (2021). Nonlinear vibration of full-filled fluid corrugated sandwich functionally

graded cylindrical shells. *Journal of Vibration and Control*, 27(9-10), 1020-1035.

[7]. H.S. Shen. (2011). Postbuckling of nanotube-reinforced composite cylindrical shells in thermal environments, Part I: axially-loaded shells. *Composite Structures,* 93(8), 2096-2108.

[8]. H.S. Shen. (2011). Postbuckling of nanotube-reinforced composite cylindrical shells in thermal environments, Part II: pressure-loaded shells. *Composite Structures*, 93(10), 2496-2503.

[9]. P.T. Hieu, H.V. Tung. (2020). Buckling of shear deformable FG-CNTRC cylindrical shells and toroidal shell segments under mechanical loads in thermal environments. *Journal of Applied Mathematics and Mechanics*, 100(11), e201900243.

[10]. Y. Kiani, R. Dimitri, F. Tornabene. (2018). Free vibration of FG-CNT reinforced composite skew cylindrical shells using the Chebyshev-Ritz formulation. *Composites Part B: Engineering*, 147, 169-177.

[11]. D.T. Dong, V.H. Nam, N.T. Phuong, L.N. Ly, V.M. Duc, N.V. Tien, T.Q. Minh, V.T. Hung, P.H. Quan. (2022). An analytical approach of nonlinear buckling behavior of longitudinally compressed carbon nanotube-reinforced (CNTR) cylindrical shells with CNTR stiffeners in thermal environment. *Journal of Applied Mathematics and Mechanics*, 102(4), e202100228.

[12]. H.S. Shen, Y. Xiang. (2018). Postbuckling behavior of functionally graded graphene-reinforced composite laminated cylindrical shells under axial compression in thermal environments. *Computer Methods in Applied Mechanics and Engineering*, 330, 64-82.

[13]. H.S. Shen, Y. Xiang. (2018). Postbuckling of functionally graded graphene-reinforced composite laminated cylindrical shells subjected to external pressure in thermal environments. *Thin-Walled Structures*, 124, 151-160.

[14]. N.T. Phuong, V.M. Duc, C.V. Doan, V.H. Nam. (2021). Nonlinear torsional buckling of functionally graded graphene-reinforced composite (FG-GRC) laminated cylindrical shells stiffened by FG-GRC laminated stiffeners in thermal environment. *Polymer Composites*, 42(6), 3051-3063.

[15]. V.H. Nam, N.T. Phuong, H.S. Lanh, V.M. Duc, C.V. Doan. (2023). Nonlinear buckling analysis of stiffened FG-GRC laminated cylindrical shells subjected to axial compressive load in thermal environment. *Mechanics Based Design of Structures and Machines*, 51(7), 3678-3694.

[16]. N.T. Phuong, N.T. Trung, C.V. Doan, N.D. Thang, V.M. Duc, V.H. Nam. (2020). Nonlinear thermomechanical buckling of FG-GRC laminated cylindrical shells stiffened by FG-GRC stiffeners subjected to external pressure. *Acta Mechanica*, 231, 5125-5144.

[17]. C. Li, J. Yang, H.S. Shen. (2022). Postbuckling of pressure-loaded auxetic sandwich cylindrical shells with FG-GRC facesheets and 3D double-V meta-lattice core. *Thin-Walled Structures*, 177, 109440.

[18]. M. Song, X. Li, S. Kitipornchai, Q. Bi, J. Yang. (2019). Low-velocity impact response of geometrically nonlinear functionally graded graphene platelet-reinforced nanocomposite plates. *Nonlinear Dynamics*, 95(3), 2333-2352.

[19]. Q. Zhou, J.H. Zhang, Y.G. Zhao. (2024). Nonlinear Buckling and Postbuckling of Circular Plates Reinforced with Graphene Platelets Using the Shooting Method. *International Journal of Structural Stability and Dynamics*, 24(01), 2450001.

[20]. V.H. Nam, T.Q. Minh, P.T. Hieu, V.T. Hung, B.T. Tu, N.T.T. Hoai, D.T. Dong. (2023). A new analytical approach for nonlinear thermo-mechanical postbuckling of FG-GPLRC circular plates and shallow spherical caps stiffened by spiderweb stiffeners. *Thin-Walled Structures*,

193, 111296.

[21]. N.T. Phuong, D.T. Dong, B.T. Tu, V.M. Duc, L.N. Khuong, P.T. Hieu, V.H. Nam. (2024). Nonlinear thermo-mechanical axisymmetric stability of FG-GPLRC spherical shells and circular plates resting on nonlinear elastic medium. *Ships and Offshore Structures*, 19(6), 820-830.

[22]. Y. Wang, R. Zeng, M. Safarpour. (2020). Vibration analysis of FG-GPLRC annular plate in a thermal environment. *Mechanics Based Design of Structures and Machines*, 50(1), 352-370.

[23]. L.K. Hoa, V.T. Hung, P.H. Quan, V.H. Nam. (2021). Nonlinear buckling and postbuckling of spiral stiffened FG-GPLRC cylindrical shells subjected to torsional loads. Journal of Science and Transport Technology, 1(1), 26-35.

[24]. J. Zhu, Z. Wang, L. Zhang, H. Wu, L. Zhao, H. Zhang, H. Wu. (2024). Wave Propagation in the Semi-Infinite Functionally Graded Porous Plates Reinforced with Graphene Platelets. *International Journal of Structural Stability and Dynamics*.

[25]. D. Liu, Y. Zhou, J. Zhu. (2021). On the free vibration and bending analysis of functionally graded nanocomposite spherical shells reinforced with graphene nanoplatelets: Three-dimensional elasticity solutions. *Engineering Structures*, 226, 111376.

[26]. Y.Q. Wang, C. Ye, J.W. Zu. (2019). Nonlinear vibration of metal foam cylindrical shells reinforced with graphene platelets. *Aerospace Science and Technology*, 85, 359-370.